

Long-time quantum simulation of the primary charge separation in bacterial photosynthesis

NANCY MAKRI[†], EUNJI SIM, DMITRII E. MAKAROV, AND MARIA TOPALER

School of Chemical Sciences, University of Illinois, 505 South Mathews Avenue, Urbana, IL 61801

Communicated by Peter G. Wolynes, University of Illinois, Urbana, IL, December 22, 1995 (received for review October 17, 1995)

ABSTRACT Accurate quantum mechanical simulations of the primary charge transfer in photosynthetic reaction centers are reported. The process is modeled by three coupled electronic states corresponding to the photoexcited chlorophyll special pair (donor), the reduced bacteriopheophytin (acceptor), and the reduced accessory chlorophyll (bridge) that interact with a dissipative medium of protein and solvent degrees of freedom. The time evolution of the excited special pair is followed over 17 ps by using a fully quantum mechanical path integral scheme. We find that a free energy of the reduced accessory chlorophyll state $\approx 400 \text{ cm}^{-1}$ lower than that of the excited special pair state yields state populations in agreement with experimental results on wild-type and modified reaction centers. For this energetic configuration electron transfer is a two-step process.

Plants and photosynthetic bacteria store energy through a series of electron transfer reactions initiated by photoexcitation of a chlorophyll dimer leading eventually to reduction of a quinone on the opposite side of the cell membrane. In spite of intense experimental and theoretical activity in the past two decades, several aspects surrounding the mechanism of photosynthesis remain elusive. For example significant controversy surrounds the role of the accessory bacteriochlorophyll during the early stages of the process.

Most recent studies have focused on bacterial photosynthetic reaction centers such as those located in the membranes of *Rhodospseudomonas viridis* (Fig. 1) or *Rhodobacter sphaeroides* because of the availability of X-ray structures for these systems (1, 2). The process begins with photoexcitation of the chlorophyll special pair, which induces a transition to the singlet state P^* of the dimer. Photoexcitation is followed by the transfer of an electron to a distant bacteriopheophytin H_L (Fig. 2) with time constant equal to about 3 ps and with quantum yield that approaches unity (3–7). It is now accepted that this fast long-range electron transfer is mediated by an accessory bacteriochlorophyll monomer B_L whose reduced state couples to those of the excited special pair and the bacteriopheophytin. However, the energetics of the accessory chlorophyll, as well as the mechanism of the process, are still under debate (5–25).

Time-resolved experiments on wild-type reaction centers (3–6) have failed to detect a reduced accessory chlorophyll state and concluded that the population of this state remains small throughout the charge transfer. If the chlorophyll monomer is involved via a sequential mechanism, this behavior is possible if the second step is much faster than the first. Fluorescence experiments have revealed a multiexponential character for the decay of the photoexcited special pair (7–9), characteristic of a two-step mechanism. An alternative interpretation is that the process follows a superexchange mechanism. In that case, deviations from simple exponential decay can still arise because the protein environment contains modes whose correlations decay extremely slowly (10). Another in-



FIG. 1. Three-dimensional view of the bacterial photosynthetic reaction center at *Rps. viridis*. Shown in red are the groups that participate in the electron transfer process.

terpretation of the nonexponential decay features of reaction centers involves an adiabatic dynamic solvation model (11, 12).

Egger and Mak (22, 23) have used quantum Monte Carlo path integral methods to simulate the initial 2 ps of the process modeled as a dissipative three-state system with an “ohmic” (26) spectral density. By exploring various parameter combinations, they concluded that dynamics compatible with the experimental findings on wild-type reaction centers can arise

The publication costs of this article were defrayed in part by page charge payment. This article must therefore be hereby marked “advertisement” in accordance with 18 U.S.C. §1734 solely to indicate this fact.

[†]To whom reprint requests should be addressed.

only if the accessory bacteriochlorophyll has energy ≈ 660 cm^{-1} below or above that of the photoexcited special pair. However, this simulation period was generally too short to establish the maximum height of the transient bridge population and its survival time.

Recent experiments by Zinth and coworkers (24, 25) on modified reaction centers (where the bacteriopheophytin has been replaced by a pheophytin of much higher free energy) have reported significant ($\approx 30\%$) long-lived populations of the reduced accessory chlorophyll. The additional information obtained from these experiments is perhaps sufficient to allow unambiguous characterization of the mechanism of bacterial photosynthesis.

We have performed accurate fully quantum mechanical simulations of the electron transfer dynamics in the wild-type and modified reaction centers of *Rb. sphaeroides* over a period of 17 ps, varying the unknown bridge free energy and the electronic couplings. Calculations for this long time interval became possible with an iterative path integral scheme recently developed in our group. The simulation interval is sufficiently long for transient populations to decay, yielding a complete picture of the dynamics free of Monte Carlo noise. The resulting electronic state populations are in good agreement with both of the above experimental observations if the reduced state of the accessory bacteriochlorophyll lies ≈ 400 cm^{-1} lower than the excited special pair and if the process is sequential. These conclusions are in accord with the theoretical analysis of Marcus (19, 20) and with the data interpretation of ref. 24 according to a simple two-step kinetic model.

METHODS

Electron transfer is a classically forbidden process requiring quantum mechanical treatment. Because of the long-range nature of the Coulomb potential, the charge transfer dynamics is strongly affected by a large number of protein and solvent coordinates. Although many protein backbone motions are slow, the presence of high-frequency vibrations suggests that the environment, too, must be treated by quantum mechanics. By virtue of the central limit theorem, the effect of the nuclear degrees of freedom should then be equivalent to that of a dissipative heat bath composed of effective harmonic modes (27–30). Indeed, the parabolic character of the free energy surfaces in electron transfer processes is central to Marcus'

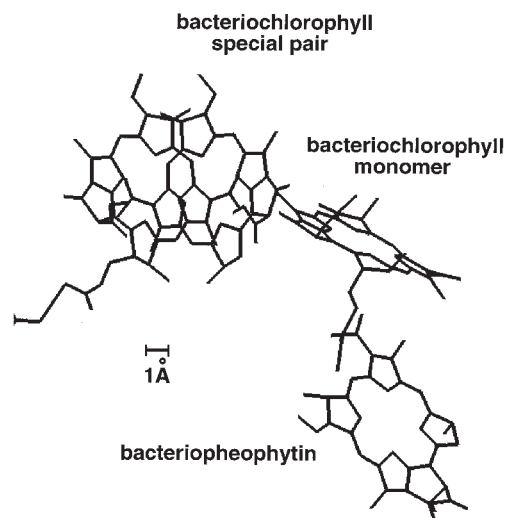


FIG. 2. Arrangement of the chlorophyll special pair, accessory chlorophyll monomer, and bacteriopheophytin in the photosynthetic reaction center of *Rps. viridis*. The center-to-center distance between the special pair and the bacteriopheophytin is ≈ 17 Å.

theory (31, 32) and has been confirmed by recent molecular dynamics simulations (21, 33). Even with this useful simplification, following the time evolution requires calculation of the quantum density matrix with a large number of coupled coordinates. Because of the delocalized nature of quantum mechanical wave functions, the numerical effort required to integrate the wave equation increases exponentially with the number of particles.

Feynman has proposed (27, 34) an alternative approach to quantum dynamics, which expresses the transition amplitude for a process as a sum of interfering amplitudes along all paths connecting the initial and final states. Because harmonic degrees of freedom enter as Gaussian variables that can be integrated out analytically, the path integral circumvents the difficult task of solving the many-body wave equation, but it requires multidimensional integration of oscillatory amplitudes that depend on the entire history of a path through solvent-induced memory interactions (35). Various attempts to evaluate the path integral by importance sampling procedures have been successful for relatively short times; integration of oscillatory functions requires effort that scales exponentially with the dimension of the integral and, therefore, with the total number N of time steps (36).

Our group has recently developed an iterative procedure for evaluating the path integral on a grid, which is accurate and stable over very long time lengths. The starting point is the observation that the memory time t_m is finite because of solvent dephasing effects that tend to destroy coherence, allowing decomposition of the N -dimensional integral for propagation through time t into N/k k -dimensional integrals where $k = t_m/\Delta t$ is the number of time steps Δt required to span the memory length (37, 38). This idea is schematically illustrated by the diagram of Fig. 3, which shows the surviving memory interactions in the evolution of the reduced density matrix. An augmented reduced density matrix \mathbf{R} [which depends on the coordinates of k time points and thus has dimension $(M^2)^k$, where M is the number of system states involved] is propagated forward in time according to the linear mapping

$$\mathbf{R}((n+1)k\Delta t) = \mathbf{T} \cdot \mathbf{R}(nk\Delta t),$$

where \mathbf{T} is an appropriate propagator matrix. After N/k iterations, \mathbf{R} is projected onto the coordinates of a single time point to yield the reduced density matrix $\tilde{\rho}(t)$ of the system. This process, combined with an improved reference potential (39), gives rise to a fully quantum mechanical scheme for obtaining the time evolution. This approach is easily feasible on desktop computers if the number of relevant system states is not very large and the solvent memory spans only a few time steps (40).

In the present case however, the protein environment is dominated by sluggish modes, and the memory length spans up to 30 time steps so that the above procedure would require storage of $(3^2)^{30} \approx 4 \times 10^{28}$ augmented reduced density matrix elements. For this reason, it was necessary to modify the above scheme to reduce the required computer storage. The crucial modification that enabled the calculations presented in Figs. 7 and 8 consists of discarding from the propagator matrix those path segments that enter in the path integral with negligible

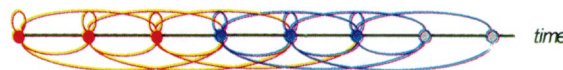


FIG. 3. Schematic representation of interactions (curved lines) in the path integral expression for the reduced density matrix. The circles indicate time points separated by Δt . Red and blue circles correspond to points defining the augmented reduced density matrix at times 0 and $k\Delta t$, respectively. The red lines indicate the interactions included in the propagator matrix.

weight. The significant path segment that are included are preselected based on their weight in the path integral from a short-time Monte Carlo random walk (41).

RESULTS

We present numerical simulations of the electron transfer dynamics in the wild-type and modified reaction centers of *Rb. sphaeroides*. In each case, our model consists of three electronic states corresponding to the photoexcited special pair and to those of the reduced accessory bacteriochlorophyll and bacteriopheophytin (or pheophytin) of the L branch. In the absence of more specific information, we have used a linear arrangement of the three diabatic surfaces with equal spatial separations between adjacent states. We adopt the following notation for these electronic states:

$$\begin{aligned} \text{State 1:} & \quad \text{P}^*\text{B}_L\text{H}_L \\ \text{State 2:} & \quad \text{P}^{*+}\text{B}_L^-\text{H}_L \\ \text{State 3:} & \quad \text{P}^{*+}\text{B}_L\text{H}_L^- \end{aligned}$$

The Hamiltonian has the form

$$H = \begin{pmatrix} E_1 & V_{12} & 0 \\ V_{12} & E_2 & V_{23} \\ 0 & V_{23} & E_3 \end{pmatrix} + \sum_j \frac{P_j^2}{2m_j} + \frac{1}{2} m_j \omega_j^2 x_j^2 + c_j x_j \begin{pmatrix} -1 & 0 & 0 \\ 0 & 0 & 0 \\ 0 & 0 & 1 \end{pmatrix}.$$

We set the free energy E_1 of the initial state equal to zero in both systems. The free energy E_2 of the accessory bacteriochlorophyll, as well as the electronic coupling V_{12} between donor and bridge, were given the same values in both systems because substitution of bacteriopheophytin by pheophytin is expected to introduce minor perturbations to the energetics of these two states. From the magnetic field dependence of the triplet state decay (42, 43), the acceptor free energy E_3 was found to be approximately equal to -2000 cm^{-1} in the case of the wild-type reaction center. The free energy of that state has been estimated to be $\approx -630 \text{ cm}^{-1}$ in the modified reaction center based on known redox potentials (24, 25). We have adopted these values in our simulations. Because the large separation ($\approx 17 \text{ \AA}$) between the chlorophyll dimer and the pheophytin results in negligible overlap of their electronic wave functions, we set the coupling V_{13} equal to zero in both systems. The energy E_2 of the reduced accessory chlorophyll state was treated as an adjustable parameter. The electronic coupling constants V_{12} and V_{23} were adjusted to yield electronic state populations similar to those inferred from the time-resolved absorbance experiments reported in ref. 24. We found that the electron transfer rate is controlled primarily by the magnitude of V_{12} , whereas V_{23} determines the transient bridge population.

The atoms of both the biomolecular units and the water environment were modeled as a harmonic heat bath whose strength of interaction with the electronic states is specified by a spectral density function that is defined as follows (26):

$$J(\omega) = \frac{\pi}{2} \sum_j \frac{c_j^2}{m_j \omega_j} \delta(\omega - \omega_j).$$

Schulten and Tesch (33), as well as Chandler and coworkers (21), have performed molecular dynamics simulations on *Rps. viridis* and obtained gap fluctuation correlation functions that can be used to calculate the bath spectral density. Xu and

Schulten (44) used the spin-boson (dissipative two-state) model to characterize the $\text{P}^* \longrightarrow \text{H}$ charge transfer. The correlation functions obtained from the above simulations differ primarily in their behavior on long times; Schulten's function decays approximately exponentially with time constant equal to 94 fs, whereas small amplitude correlations that were persistent on long time scales emerged from Chandler's simulations.

Our calculations used two spectral density functions that correspond to different parameterizations in the work of Chandler and coworkers: the first (hereafter *spectral density I*) was obtained from an approximate fit of ohmic form (26) ($J(\omega) \sim \omega e^{-\omega/\omega_c}$) to the spectral density of model I in ref. 21, which was obtained from molecular dynamics simulations of the reaction center of *Rps. viridis*. The second (*spectral density II*) is the exact spectral density calculated from molecular dynamics simulations with model II in the same work, which included (in addition to the biological units) crystallization water molecules treated as simple point charges. These two spectral densities are depicted in Fig. 4. Whereas the integral of $J(\omega)/\omega$ is set equal to the solvent reorganization energy (estimated to be 2000 cm^{-1} in both cases so that the free energy surfaces for the donor and acceptor intersect at the activationless geometry in the case of the wild-type reaction center), low frequencies are more heavily weighted in spectral density II. Fig. 5 shows the corresponding response functions whose decay characteristics determine the memory length in the path integral. The response function drops off very slowly in the case of spectral density II, and the memory length is expected to be long in this case, presenting a challenge to our iterative path integral scheme. Finally, correlations on very long time scales (on the order of tens of picoseconds) are not described accurately by either of these molecular dynamics-based spectral densities, but they have been estimated to account for a significant fraction of the medium reorganization energy (45). We believe that the omission of such long-time correlations does not affect the basic conclusions of the present work which are based on

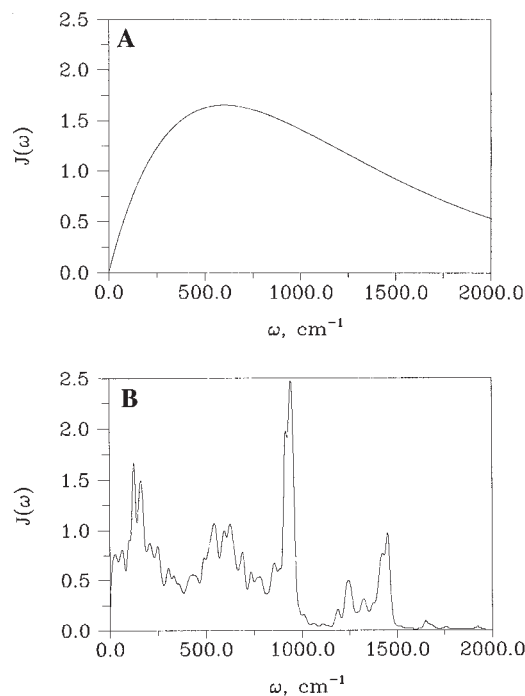


FIG. 4. Spectral densities employed in the quantum simulations. (a) Spectral density I, obtained from an approximate ohmic fit to the data of model I in ref. 5. (b) Spectral density II, the function calculated by Chandler and coworkers from molecular dynamics simulations with the parameters of model II.

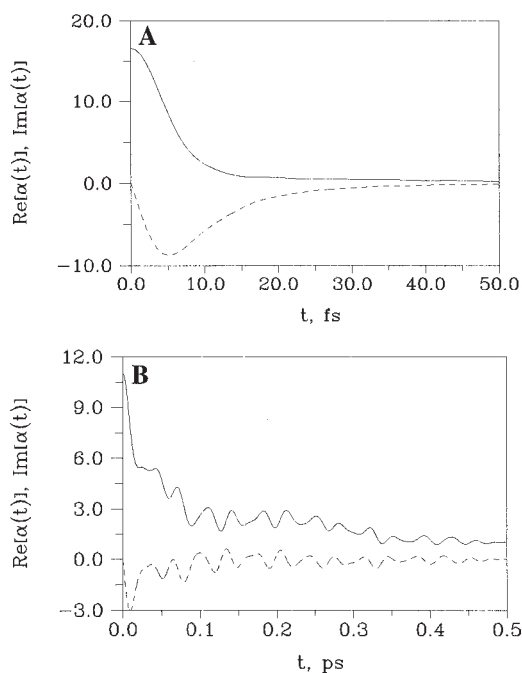


FIG. 5. Solvent response functions at 300 K for the two spectral densities depicted in Fig. 4. Solid and dashed lines correspond to real and imaginary parts, respectively.

the magnitude of the electronic state populations, although it may prevent observation of nonexponential features in the time-dependence of each single-step event.

The geometry change for the $P \rightarrow P^*$ transition is not known, but there is evidence from absorption and emission spectra (46) that vertical excitation results in appreciable excess vibrational energy above that of the excited state potential minimum. We have chosen an initial state where the nuclei are displaced from their equilibrium positions by amounts that add to 500 cm^{-1} of vibrational energy. The solvent rearranges rapidly in the simulation with spectral density I, while the larger contribution of low frequency modes in spectral density II causes slower relaxation on a time scale similar to that for electron transfer. In that case, State 1 appears during the initial 1–2 ps to have a higher energy, affecting the overall charge transfer rate as well as the transient bridge population.

Because the reduced bacteriochlorophyll monomer is not the final product in the early stages of charge separation, the free energy of this state must be higher than that of State 3, i.e., $E_2 > -630 \text{ cm}^{-1}$. We have performed simulations of the electron transfer process with values of E_2 ranging from -630 to $+200 \text{ cm}^{-1}$ using both spectral densities. For each value of the bridge free energy, we determined the values of electronic couplings that yield lifetime and populations compatible with the experimental results reported for the wild-type and the modified reaction centers. Significant ($\approx 30\%$) bridge population in the modified reaction center surviving over tens of picoseconds is possible only if $E_2 \approx -400 \text{ cm}^{-1}$, while the electronic coupling $V_{12} \approx 22 \text{ cm}^{-1}$ produces in both systems at room temperature lifetimes of the photoexcited special pair around 3 ps, consistent with the experimental results. For a given ratio of electronic couplings, the presence of strongly coupled low frequency modes in spectral density II leads to somewhat higher transient bridge population compared with that arising when spectral density I is used. We find that sizable population accumulates on the bacteriochlorophyll monomer within about 1 ps after photoexcitation unless $V_{23} > 6V_{12}$. Such large ratios of the two electronic couplings are in good agreement with the theoretical estimate of ref. 47. Restriction

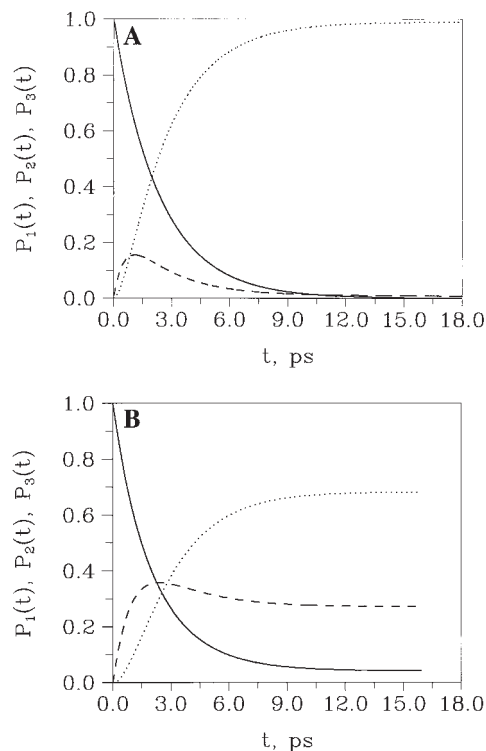


FIG. 6. Populations of the three electronic states at 300 K from the path integral calculation with spectral density I. Shown are results with optimal parameters, $E_2 = -400 \text{ cm}^{-1}$ and $V_{12} = 22 \text{ cm}^{-1}$. Solid, dashed, and dotted lines show the populations of the photoexcited special pair, the reduced bacteriochlorophyll monomer, and the reduced bacteriopeophytin or pheophytin, respectively. (a) Wild-type reaction center, $V_{23} = 135 \text{ cm}^{-1}$. (b) Modified reaction center, $V_{23} = 22 \text{ cm}^{-1}$.

of the coupling ratio to smaller values results in large bridge population and led to dismissal of similar configurations by Egger and Mak (22). Alternatively, the transient bridge population may remain small with smaller ratios of electronic couplings if the donor–acceptor reorganization energy is not partitioned equally between the two pairs of electron transfer states; this situation corresponds to a nonlinear arrangement of the diabatic surfaces (48) and is under consideration by Fleming's group (private communication). The electronic populations of the modified reaction center are qualitatively insensitive to the value of V_{23} as long as the latter is at least as large as V_{12} . Results representative of these simulations are shown in Figs. 6 and 7. The asymptotic values of these populations are in very good agreement with the thermodynamic occupation numbers obtained from Monte Carlo equilibrium path integral calculations.

Values of the bridge free energy that are higher than -400 cm^{-1} can lead to appreciable transient population of that state, particularly if the electronic coupling to the third state is small. This is true even if the bridge lies above the excited special pair because of the slow relaxation of the medium Franck–Condon energy, which keeps the donor at a higher effective energy over a period roughly equal to the relaxation time of the bath. Typical simulation results using spectral density II are presented in Fig. 8 for $E_2 = +200 \text{ cm}^{-1}$. The subsequent decay (within about 10 ps) of the bridge population to its thermal equilibrium value leads to the conclusion that positive values of the bridge energy are not compatible with the recent observation of significant long-lived bridge population in modified reaction centers.

DISCUSSION

Within the three-state description and with the solvent spectral densities described above, the results presented in Figs. 6–8 are

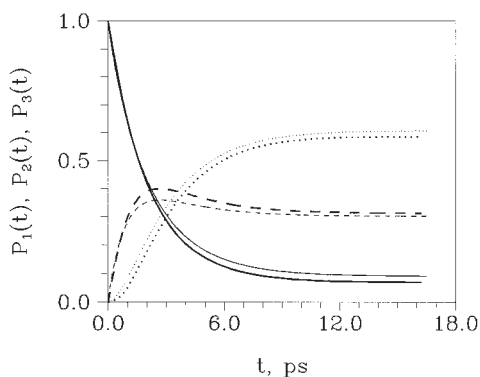
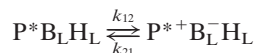
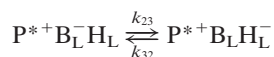


FIG. 7. Populations of the three electronic states of the modified reaction center at 300 K. The parameters are $E_2 = -400 \text{ cm}^{-1}$, $V_{12} = 22 \text{ cm}^{-1}$, $V_{23} = 22 \text{ cm}^{-1}$. Heavy solid, dashed, and dotted lines show the populations of the photoexcited special pair, the reduced bacteriochlorophyll monomer, and the reduced pheophytin, respectively, obtained from the path integral calculation with spectral density II. Thin lines show populations obtained from the two-step kinetic equation with the procedure described in the text.

accurate to 5%. These results show that a value of approximately -400 cm^{-1} for the energy of the reduced bacteriochlorophyll state is fully compatible with the experimental observations on wild-type and modified reaction centers. If indeed the first three electronic states relevant to photosynthetic electron transfer are arranged in order of decreasing energy, the process is expected to follow a two-step mechanism. To confirm this assertion, we extracted forward rate constants k_{12} and k_{23} for the two single-step reactions



and



by following the quantum time evolution of these two-level systems. The backward rate constants were obtained from the detailed balance condition. The populations corresponding to the solution of the two-step kinetic equation

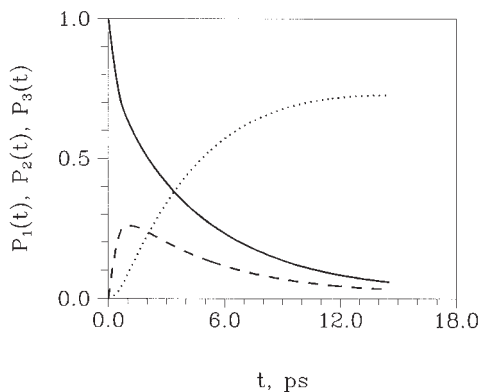


FIG. 8. Electronic state populations at 300 K in the case of the modified reaction center for an intermediate bridge energy, $E_2 = +200 \text{ cm}^{-1}$. The electronic couplings are $V_{12} = V_{23} = 30 \text{ cm}^{-1}$. Solid, dashed, and dotted lines show the populations of the photoexcited special pair, the reduced bacteriochlorophyll monomer, and the reduced pheophytin, respectively, obtained from the path integral calculation with spectral density II.

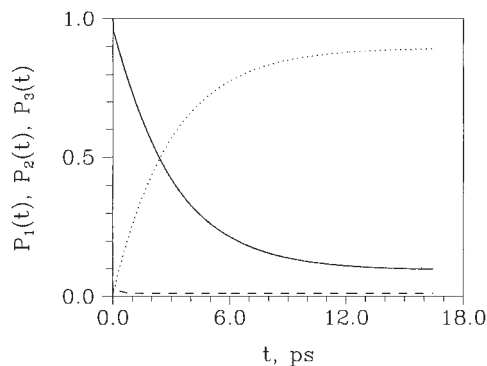
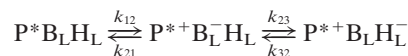
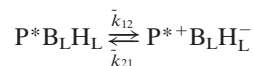


FIG. 9. Electronic state populations at 300 K in the case of the modified reaction center for a high-lying bridge state, $E_2 = +2000 \text{ cm}^{-1}$. The electronic couplings are $V_{12} = V_{23} = 240 \text{ cm}^{-1}$. Solid, dashed, and dotted lines show the populations of the photoexcited special pair, the reduced bacteriochlorophyll monomer, and the reduced pheophytin, respectively, obtained from the path integral calculation with spectral density I.



displayed in Fig. 7 for the case of the modified reaction center are seen to be in very good agreement with the calculated quantum dynamics, in accord with ref. 24. In contrast, use of the super-exchange model (19)



leads with these parameters to transfer rates that are too low by about two orders of magnitude. These conclusions are in harmony with the theoretical analysis of Marcus (19, 20).

If $V_{23} > V_{12}$, the first two-state reaction constitutes the rate-limiting step in both cases. In this parameter regime, the quantum mechanical rate for a two-level system is nearly temperature independent over a fairly broad range of temperatures, exhibiting a small decrease with increasing temperature. This observation, which is confirmed by full three-state simulations at different temperatures, provides a simple explanation of the observed weak inverted temperature dependence of the electron transfer rate in bacterial reaction centers (5). We have not carried out simulations at very low temperatures because the expected glassy behavior of the medium in that regime is likely to invalidate the particular system-bath model that we use.

We have also studied the evolution that results when the free energy of the bridge is much larger than that of the photoexcited special pair using spectral density I. With the coupling constants chosen to give $\text{P}^*\text{H}_L \rightarrow \text{P}^{*+}\text{H}$ electron transfer in the modified reaction center with time constant of $\approx 3 \text{ ps}$, the population of the accessory chlorophyll remained very small ($< 5\%$) in all simulations with $E_2 > 500 \text{ cm}^{-1}$ because of overwhelming Boltzmann factors. A typical result is presented in Fig. 9 for $E_2 = +2000 \text{ cm}^{-1}$. With this spectral density, positive values of the bridge free energy can give rise to appreciable bridge population only if the electronic coupling to the excited special pair is sufficiently large to mix these states, i.e., on the order of E_2 . Because it is very unlikely[‡] that V_{12} is as large as 10^3 cm^{-1} , we conclude that the model using spectral density I rules out electronic configurations where the bridge energy lies above that of P^* . Non-negligible transient population of the accessory chlorophyll may arise with a high-lying bridge state via a two-step process if the low-

[‡]In fact, Warshel *et al.* (7) have estimated this coupling to be of the order of 10^1 cm^{-1} .

frequency spectral density II is employed and the Franck-Condon displacement in the excited electronic state is large. However, this population would be short-lived (qualitatively similar to that displayed in Fig. 8) and cannot explain the spectroscopic data that indicate significant bridge population over hundreds of picoseconds. Of course, as we have not performed simulations with spectral density II for high-lying bridge configurations, a super-exchange mechanism cannot be entirely ruled out, although we consider it unlikely.

N.M. thanks Prof. David Chandler for drawing her attention to this problem and for useful comments on the manuscript. We also thank Prof. Peter Wolynes for many stimulating discussions. This work has been supported by a Young Investigator Award and Grant No. CHE 93-13603 from the National Science Foundation, a Beckman Young Investigator Award, and a Packard Fellowship for Science and Engineering.

1. Deisenhofer, J., Epp, O., Miki, K., Huber, R. & Michel, H. (1984) *J. Mol. Biol.* **180**, 385–398.
2. Deisenhofer, J., Epp, O., Miki, K., Huber, R. & Michel, H. (1985) *Nature (London)* **318**, 618–624.
3. Martin J. L., Breton, J., Hoff, A. J., Migus, A. & Antonetti, A. (1986) *Proc. Natl. Acad. Sci. USA* **83**, 957–961.
4. Breton, J., Martin, J. L., Migus, A., Antonetti, A. & Orszag, A. (1986) *Proc. Natl. Acad. Sci. USA* **83**, 5121–5125.
5. Fleming, G. R., Martin, J. L. & Breton, J. (1988) *Nature (London)* **333**, 190–192.
6. Chan, C.-K., DiMugno, T. J., Chen, L. X.-Q., Norris, J. R. & Fleming, G. R. (1991) *Proc. Natl. Acad. Sci. USA* **88**, 11202–11206.
7. Du, M., Rosenthal, S. J., Xie, X., DiMugno, T. J., Schmidt, M., Hanson, D. K., Schiffer, M., Norris, J. R. & Fleming, G. R. (1992) *Proc. Natl. Acad. Sci. USA* **89**, 8517–8521.
8. Wang, Z., Pearlstein, R. M., Jia, Y. & Fleming, G. R. (1993) *Chem. Phys.* **176**, 421–425.
9. Jia, Y., DiMugno, T. J., Chan, C.-K., Wang, Z., Du, M., Hanson, D. K., Schiffer, M. A., Norris, J. R., Fleming, G. R. & Popov, M. S. (1993) *J. Phys. Chem.* **97**, 13180–13191.
10. Gehlen, J., Marchi, M. & Chandler, D. (1994) *Science* **263**, 499–502.
11. Peloquin, J. M., Williams, J., Lin, X., Aldon, R., Taguchi, A., Allen, J. & Woodbury, N. (1994) *Biochemistry* **33**, 8089–8100.
12. Woodbury, N., Peloquin, J. M., Aldon, R., Lin, X., Lin, S., Taguchi, A., Williams, J. & Allen, J. (1994) *Biochemistry* **33**, 8101–8112.
13. Bixon, M., Jortner, J., Michel-Beyerle, M. E., Ogrodnik, A. & Lersch, W. (1987) *Chem. Phys. Lett.* **140**, 626–630.
14. Bixon, M., Jortner, J. & Michel-Beyerle, M. E. (1991) *Biochim. Biophys. Acta* **1056**, 301–315.
15. Michel-Beyerle, M. E., Plato, M., Deisenhofer, J., Michell, H., Bixon, M. & Jortner, J. (1988) *Biochim. Biophys. Acta* **933**, 52–70.
16. Friesner, R. A. & Won, Y. (1989) *Biochim. Biophys. Acta* **977**, 99.
17. Warshel, A., Creighton, S. & Parson, W. W. (1988) *J. Phys. Chem.* **92**, 2696–2701.
18. Creighton, S., Hwang, J. K., Warshel, E., Parson, W. W. & Norris, J. (1988) *Biochemistry* **27**, 774–781.
19. Marcus, R. A. (1987) *Chem. Phys. Lett.* **133**, 471–477.
20. Marcus, R. A. (1988) *Chem. Phys. Lett.* **146**, 13–21.
21. Marchi, M., Gehlen, J. N., Chandler, D. & Newton, M. (1993) *J. Am. Chem. Soc.* **115**, 4178–4190.
22. Egger, R. & Mak, C. H. (1994) *J. Phys. Chem.* **98**, 9903–9918.
23. Mak, C. H. & Egger, R. (1995) *Chem. Phys. Lett.* **238**, 149–157.
24. Schmidt, S., Arlt, T., Hamm, P., Huber, H., Nagele, T., Wachtveitl, J., Meyer, M., Scheer, H. & Zinth, W. (1994) *Chem. Phys. Lett.* **223**, 116–120.
25. Huber, H., Meyer, M., Nagele, T., Hartl, I., Scheer, H., Zinth, W. & Wachtveitl, J. (1995) *Chem. Phys.* **197**, 297–305.
26. Leggett, A. J., Chakravarty, S., Dorsey, A. T., Fisher, M. P. A., Garg, A. & Zwirger, M. (1987) *Rev. Mod. Phys.* **59**, 1–85.
27. Feynman, R. P. & Hibbs, A. R. (1965) *Quantum Mechanics and Path Integrals* (McGraw-Hill, New York).
28. Onuchic, J. N. & Wolynes, P. G. (1988) *J. Phys. Chem.* **92**, 6495–6503.
29. Onuchic, J. N. & Wolynes, P. G. (1993) *J. Chem. Phys.* **98**, 2218–2224.
30. Marcus, R. A. (1993) *Angew. Chem. Int. Ed. Engl.* **32**, 1111–1121.
31. Marcus, R. A. (1956) *J. Chem. Phys.* **24**, 966–979.
32. Marcus, R. A. & Sutin, N. (1985) *Biochim. Biophys. Acta* **811**, 265–322.
33. Schulten, K. & Tesch, M. (1991) *Chem. Phys.* **158**, 421–446.
34. Feynman, R. P. (1948) *Rev. Mod. Phys.* **20**, 367–387.
35. Feynman, R. P. & Vernon, F. L., Jr. (1963) *Ann. Phys.* **24**, 118–173.
36. Makri, N. (1991) *Comp. Phys. Commun.* **63**, 389–414.
37. Makarov, D. E. & Makri, N. (1994) *Chem. Phys. Lett.* **221**, 482–491.
38. Makri, N. & Makarov, D. E. (1995) *J. Chem. Phys.* **102**, 4600–4610.
39. Makri, N. (1992) *Chem. Phys. Lett.* **193**, 435–444.
40. Makri, N. (1995) *J. Math. Phys.* **36**, 2430–2457.
41. Sim, E. & Makri, N. (1996) *Chem. Phys. Lett.* **249**, 224–230.
42. Goldstein, R. A., Takiff, L. & Boxer, S. G. (1988) *Biochim. Biophys. Acta* **934**, 253–263.
43. Chidsey, C. E. D., Takiff, L., Goldstein, R. A. & Boxer, S. G. (1985) *Proc. Natl. Acad. Sci. USA* **82**, 6850–6854.
44. Xu, D. & Schulten, K. (1994) *Chem. Phys.* **182**, 91–117.
45. Gehlen, J. N. (1994) Ph.D. thesis (Univ. of California, Berkeley).
46. Leguit, L., Visschers, R. W., Crielaard, W., van Grondelle, R. & Hellingerwerf, K. J. (1992) *Biochim. Biophys. Acta* **1102**, 177–185.
47. Plato, M., Mobius, K., Michel-Beyerle, M. E., Bixon, M. & Jortner, J. (1988) *J. Am. Chem. Soc.* **110**, 7279–7285.
48. Cho, M. & Silbey, R. (1995) *J. Chem. Phys.* **103**, 593.